

Cite this: *Nanoscale Horiz.*, 2024,  
9, 1250

## Catalyst durability in electrocatalytic H<sub>2</sub>O<sub>2</sub> production: key factors and challenges†

Ji Sik Choi,<sup>ab</sup> Guilherme V. Fortunato,<sup>id</sup>\*<sup>abc</sup> Daniele C. Jung,<sup>id</sup><sup>a</sup>  
Julio C. Lourenço,<sup>id</sup><sup>bc</sup> Marcos R. V. Lanza<sup>c</sup> and Marc Ledendecker<sup>\*bd</sup>

On-demand electrocatalytic hydrogen peroxide (H<sub>2</sub>O<sub>2</sub>) production is a significant technological advancement that offers a promising alternative to the traditional anthraquinone process. This approach leverages electrocatalysts for the selective reduction of oxygen through a two-electron transfer mechanism (ORR-2e<sup>-</sup>), holding great promise for delivering a sustainable and economically efficient means of H<sub>2</sub>O<sub>2</sub> production. However, the harsh operating conditions during the electrochemical H<sub>2</sub>O<sub>2</sub> production lead to the degradation of both structural integrity and catalytic efficacy in these materials. Here, we systematically examine the design strategies and materials typically utilized in the electroproduction of H<sub>2</sub>O<sub>2</sub> in acidic environments. We delve into the prevalent reactor conditions and scrutinize the factors contributing to catalyst deactivation. Additionally, we propose standardised benchmarking protocols aimed at evaluating catalyst stability under such rigorous conditions. To this end, we advocate for the adoption of three distinct accelerated stress tests to comprehensively assess catalyst performance and durability.

Received 12th March 2024,  
Accepted 29th May 2024

DOI: 10.1039/d4nh00109e

rsc.li/nanoscale-horizons

### 1. Introduction

Electrochemical devices powered by sustainable energy sources offer certain advantages over traditionally fossil fuel-based chemical production methods as they can be operated on-demand and in a decentralized manner.<sup>1,2</sup> At the heart of the technology are electrocatalysts facilitating electrochemical reactions by providing pathways for electrons to move between electrodes and reactants.<sup>3</sup> Seen as a significant technological advancement for many industrial, commercial and domestic end-users, the on-demand electrocatalytic hydrogen peroxide (H<sub>2</sub>O<sub>2</sub>) production has gained significant attention as a promising alternative to the traditional anthraquinone process. The former process involves the selective 2-electron oxygen-reduction (ORR-2e<sup>-</sup>) and a multitude of active and selective catalysts have been proposed in literature enabling on-demand H<sub>2</sub>O<sub>2</sub> electrosynthesis.<sup>4,5</sup> However, the critical aspect of stability,

crucial for industrial viability, is frequently overlooked or inadequately assessed, if considered at all.

Catalyst performance and degradation processes can significantly vary based on the reaction environment and the specific catalyst used particularly due to the low pH values, negative applied potentials and current densities.<sup>6</sup> Here, we methodically explore commonly employed materials and design strategies for the electroproduction of H<sub>2</sub>O<sub>2</sub> under low pH conditions. In order to understand the conditions, the catalysts have to overcome, we delve into currently discussed reactor configurations and analyse the factors that lead to catalyst deactivation. By doing so, we present standardised benchmarking protocols intended to evaluate catalyst stability in these demanding environments.

### 2. Electrocatalysts for H<sub>2</sub>O<sub>2</sub> production

Given the extensive array of electrocatalysts available for hydrogen peroxide production, our initial focus is on introducing the catalysts most frequently utilised in the acidic oxygen reduction reaction for generating H<sub>2</sub>O<sub>2</sub>. The most commonly used catalyst materials are displayed in Fig. 1(B) and (C). As these catalysts exhibit diverse intrinsic properties, the prevalence of distinct degradation mechanisms is strongly influenced by the specific catalytic material in use. In general, the main classes of electrocatalysts for H<sub>2</sub>O<sub>2</sub> production include metal-free carbon-based

<sup>a</sup> Department of Technical Chemistry, Technical University of Darmstadt, Peter-Grünberg-Straße 8, 64287 Darmstadt, Germany. E-mail: g.fortunato@tum.de

<sup>b</sup> Sustainable Energy Materials, Technical University Munich, Campus Straubing, Schulgasse 22, 94315 Straubing, Germany. E-mail: marc.ledendecker@tum.de

<sup>c</sup> São Carlos Institute of Chemistry, University of São Paulo, Avenida Trabalhador São-Carlense 400, São Carlos, SP 13566-590, Brazil

<sup>d</sup> Helmholtz Institute Erlangen-Nürnberg for Renewable Energy (IEK-11), Forschungszentrum Jülich GmbH, Cauerstr. 1, 91058 Erlangen, Germany

† Electronic supplementary information (ESI) available. See DOI: <https://doi.org/10.1039/d4nh00109e>





**Fig. 1** Catalysts and strategies for oxygen reduction reaction optimisation. (A) Mechanism of oxygen reduction reaction leading to the formation of both  $H_2O_2$  and  $H_2O$ . Commonly utilized catalysts include (B) carbon-based catalysts, which consist of (doped) carbonaceous materials, and (C) metal-based materials typically supported on high surface area carbon substrates. The different strategies to mitigate overreduction to  $H_2O$  encompass site blocking by adsorption or surface coverage, altering the interparticle distance, using single atoms and alloyed nanoparticles as well as altering the binding energies by metal-support interactions.

materials and transition metal-based materials that are usually supported on carbon. In acidic environments, platinum group metal electrocatalysts in particular Pt and Pd based, demonstrated the highest ORR exchange current densities.<sup>5</sup> However, extended surfaces cleave the O–O bond, following a  $4e^-$  pathway toward water production as shown in Fig. 1(A). To achieve selective ORR- $2e^-$ , active sites have been isolated, preventing neighbouring sites from splitting the O–O bond. One approach to create these isolated active sites involves blending active metals, such as Pt and Pd, with metals possessing low oxygen affinity, such as Hg, Au, or Ag.<sup>4,7,8</sup> Even though the specific nature of metal/metal interactions is occasionally ambiguous. In the case of the Pt/Hg system, Hg is electrodeposited on the Pt surface while in other cases solid solutions are formed. In all cases, the employed metal composition is rather poor in the active metal such as Pt or Pd in order to prevent overreduction to  $H_2O$ .

Active suppression of  $H_2O_2$  re-adsorption through control of overall metal loading<sup>9–13</sup> and interparticle distance<sup>12</sup> has resulted in selectivities exceeding 90% in a rotating ring disk electrode configuration. Another approach is blocking Pt or Pd active sites using less active materials, for example, amorphous carbon,<sup>14</sup> polymers,<sup>15,16</sup> oxides,<sup>17</sup> and polyatomic ions<sup>18</sup> to achieve similar isolation of active sites. Equally, atomically dispersed metal sites, known as single-atom catalysts (SACs), supported on inert substrates have been proposed, where the coordination environment of the support matrix can tune the catalytic activity and selectivity.<sup>19–24</sup> The trend towards downsizing metal catalysts from extended surfaces to isolated single-atom sites necessitates a meticulous re-evaluation of the metal-support interaction. As particle size shrinks, the interface between the metal and the support becomes increasingly dominant, significantly impacting catalyst activity and stability.<sup>25</sup> This is critical since lower-coordinated metal atoms in a

nanoparticle exhibit increased surface energy, making them more susceptible to degradation mechanisms such as dissolution and Ostwald ripening.<sup>26–28</sup> For SACs, precisely controlling the interaction between the isolated metal atoms and the supporting material is paramount. This strong metal-support interaction directly governs the stability of the catalyst, the nature of its active sites, and ultimately the types of reactions it can facilitate.

When doped with nitrogen, sulfur, or oxygen, carbon supports enhance the physicochemical properties of catalysts by improving nanoparticle dispersion and stabilising single atoms during durability tests.<sup>21,29–31</sup> These functional groups enable both, noble and non-noble metals such as Co, Ni, or Fe to remain stable in acidic media.<sup>32–34</sup> For instance, Jiajun *et al.* maintained about 70% selectivity for  $O_2$  to  $H_2O_2$  conversion with a Pt-S-CNT catalyst over 500 minutes of continuous electrolysis at  $10 \text{ mA cm}^{-2}$ , with 0.4 ppb Pt leaching as confirmed by ICP-MS.<sup>35</sup> The role of  $CoN_4$  coordination structures in the ORR pathway continues to be a subject of debate.<sup>34,36,37</sup> Chen *et al.* found that pyrrole-type  $CoN_4$  primarily supports the ORR- $2e^-$ , maintaining stability for 90 hours at  $-50 \text{ mA}$  in a flow cell, while pyridine-type  $CoN_4$  catalyzes the ORR- $4e^-$ . After stability testing, X-ray diffraction and electron microscopy analyses detected no Co nanoparticle aggregation.<sup>38</sup> Huang *et al.* enhanced the long-term stability of a diatomic cobalt catalyst by integrating a second metal into cobalt's coordination sphere, achieving stability for 100 h at current densities of  $400 \text{ mA cm}^{-2}$  in a flow cell, optimising the binding strength of critical  $H_2O_2$  intermediates.<sup>39</sup>

Bare carbon-based materials have been reported to be highly selective for ORR- $2e^-$ ,<sup>4,7,40–42</sup> though their activity is low, likely due to the weak interaction between carbon and  $*OOH$ . To boost the activity of carbon catalysts, additional treatments are effective, such as incorporating anthraquinone molecules,<sup>43,44</sup> trying to emulate the anthraquinone process, or functionalizing carbon with nitrogen or oxygen groups.<sup>45–48</sup> Oxidized or nitrogen-doped versions of carbon materials such as carbon black, carbon nanotubes, mesoporous carbon, and graphene, distinguished by their large surface areas and defect-rich structures, exhibit enhanced oxygen adsorption and activation, significantly boosting their catalytic efficacy compared with undoped carbon materials. While designated as “metal-free” catalysts, there is a high likelihood that these entities serve as anchor sites for prevalent transition metals such as iron, likely contributing to the overall activity.

It becomes clear that there is a plethora of material combinations that react to the applied reaction conditions. In electrocatalysis, degradation mechanisms are influenced by the applied conditions and the specific catalyst employed. Often, a mix of various degradation phenomena contributes to the observed overall deactivation, causing a loss in both catalytic activity and selectivity.<sup>6</sup> The degradation mechanisms thereby heavily rely on the conditions the catalyst material faces which vary based on the electrochemical device being used. For more comprehensive insights on degradation pathways influenced by operating conditions and intrinsic material properties, readers



may refer to other reviews.<sup>6,49–52</sup> Operando techniques paired with a modified scanning flow cell system, including methods like ICP-MS, DEMS, Mössbauer spectroscopy, and Raman spectroscopy, can significantly enhance our understanding of the factors that influence catalyst degradation.<sup>53–59</sup> In the subsequent section, we will present various configurations documented in literature and explore the potential conditions that the catalysts must withstand.

### 3. Identifying driving forces for catalyst deactivation in devices used for electroynthesis of hydrogen peroxide

The electroproduction of  $\text{H}_2\text{O}_2$  can be achieved in a variety of environments ranging from acidic, neutral, and alkaline media. However, the production in high pH media is less favourable, as the deprotonated form of hydrogen peroxide ( $\text{HO}_2^-$ ) must be utilized immediately, limiting its storage capabilities and reducing its applicability.<sup>60,61</sup> In the following discussion, we will focus on acidic media. Cation exchange membrane  $\text{H}_2\text{O}_2$  fuel cells ( $\text{H}_2\text{O}_2$ -FC) stand out as a leading electrochemical cell, fulfilling a dual role: generating electricity while also yielding  $\text{H}_2\text{O}_2$  as a valuable by-product.<sup>62,63</sup> Initially employing  $\text{O}_2$ -saturated liquid electrolytes on the cathode side as illustrated in Fig. 2(A), these cell designs face limitations such as low current densities restricted to a few  $\text{mA cm}^{-2}$ , resulting in

modest  $\text{H}_2\text{O}_2$  accumulation at the  $\mu\text{M}$  per hour-scale.<sup>62</sup> Efficient cell designs, which minimise the catalyst's exposure to generated peroxide, play a pivotal role in preventing unwanted side reactions that may consume the produced  $\text{H}_2\text{O}_2$  and in extending the catalyst's lifespan, as will be shown later. It is feasible to generate significant amounts of  $\text{H}_2\text{O}_2$  employing solid electrolytes and gas diffusion electrodes (Fig. 2(B)), with current densities reaching hundreds of  $\text{mA cm}^{-2}$ .

The potential applied poses a significant challenge to the catalyst's stability, particularly during start-stop. The operational potential, which must theoretically be lower than  $0.7 V_{\text{RHE}}$ , depends on the catalyst's activity,<sup>66</sup> whereas the open circuit potential (OCP) can reach potentials around  $0.9 V_{\text{RHE}}$ , particularly for Pt- and Pd-based catalysts.<sup>67,68</sup> The oscillation between operational potentials and OCP over time is expected to degrade the catalyst leading to electrocatalytic losses or changes in selectivity due to processes such as (transient) dissolution or leaching of the catalytic metal sites, support dissolution, detachment, or particle agglomeration.<sup>69–72</sup> Non-noble metals such as Ni, Co, Mo, or W have been reported to be prone to dissolution at OCP upon uncontrolled immersion into the electrolyte.<sup>73</sup>

Potential challenges may encompass catalyst poisoning, which can be intensified depending on the electrochemical device used, for example, when another oxidation reaction on the anode side is used such as *e.g.*, methanol or formic acid oxidation instead of HOR. Here, fuel crossover or contaminants

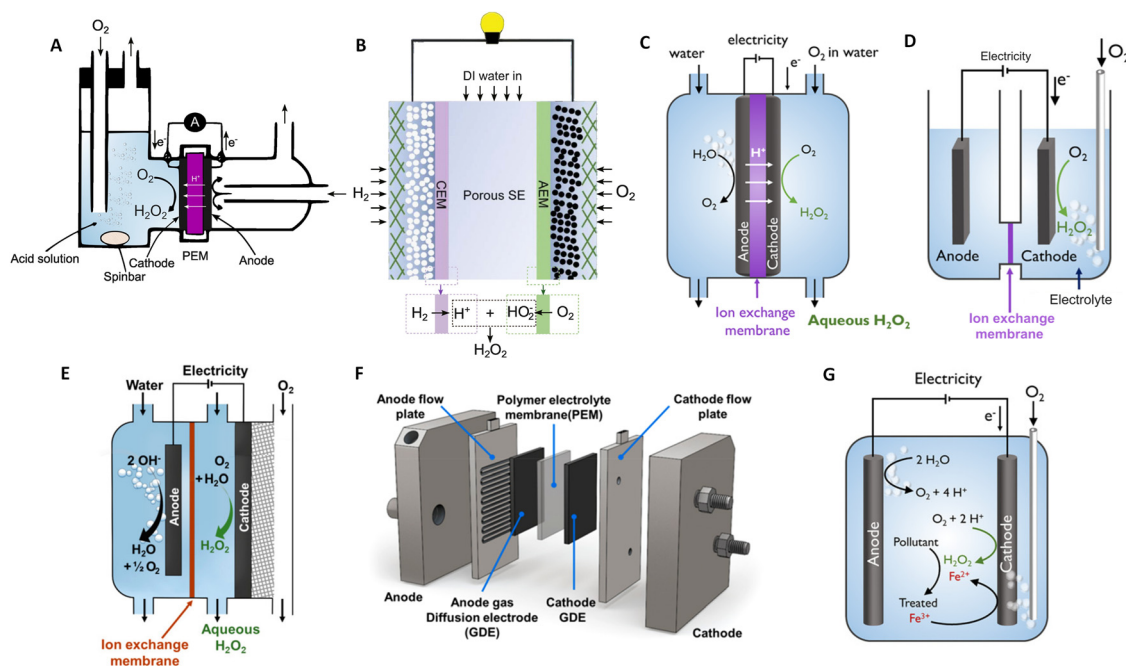


**Fig. 2** Schematic illustrations of  $\text{H}_2\text{O}_2$ -fuel cell and  $\text{H}_2\text{O}_2$ -electrolyser devices. (A) Liquid electrolyte-containing fuel cell. (B) Solid-electrolyte fuel cell with double membrane. (C) PEM electrolyser with submerged membrane electrode assembly (MEA). (D) H-cell with submerged electrodes. (E) Continuous flow reactor utilizing a gas diffusion electrode (GDE). (F) MEA-based flow reactor with a GDE anode and GDE cathode. (G) Non-dividing cell reactor for the electro-Fenton process. Panel A is adapted from ref. 62, Copyright 1990, with permission from Elsevier. Panel B is adapted from ref. 64, Copyright 2019, American Association for the Advancement of Science. Panels C, D, and G are adapted with permission from ref. 61, Copyright 2018, American Chemical Society. Panel E and F are adapted with permission from ref. 65, Copyright 2020, American Chemical Society.



such as sulphur or CO can adsorb onto the catalyst surface, blocking active sites and reducing the catalyst's activity or completely inhibiting its function.<sup>6,74</sup>

Elevated temperatures of up to 80 °C increase the rate of deactivation, leading to higher increased catalyst and/or support dissolution rates and particle detachment. This can result in a diminished activity and a reduced lifespan for the catalyst.<sup>71,72,75,76</sup>

An alternative approach for prominent production method involves the synthesis of H<sub>2</sub>O<sub>2</sub> through an electrolytic cell as shown in Fig. 2(C)–(G). As an example, within a polymer electrolyte membrane (PEM) electrolyser, the anode and cathode catalyst layer directly interface with a solid electrolyte membrane. Flow-by-reactors, which facilitate continuous H<sub>2</sub>O<sub>2</sub> extraction to limit the exposure of the catalytic layer to the generated peroxide (Fig. 2(E) and (F)) have been conceptualised and made their way into commercial applications.<sup>77</sup> Non-divided cell reactors have been proposed for the Electro-Fenton process for wastewater treatment (Fig. 2(G)). With a non-divided cell configuration, both the anode and cathode can, directly and indirectly, contribute to the degradation of pollutant molecules, offering a promising solution for the environmentally friendly treatment of wastewater contaminants.

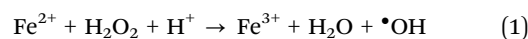
Regarding the applied potentials, the catalyst in an electrolyser is exposed to lower applied potentials (below 0 V<sub>RHE</sub>) compared to a H<sub>2</sub>O<sub>2</sub>-FC, especially when high H<sub>2</sub>O<sub>2</sub>-generation current density is required. Considering only Butler–Volmer kinetics, potentials below 0 V<sub>RHE</sub> are expected from Tafel extrapolations.<sup>64,75,78–80</sup> Conversely, the upper potential limit at the cathode should remain around OCP, similar to the conditions experienced by H<sub>2</sub>O<sub>2</sub>-FC systems. Higher potentials due to local fuel starvation will not be considered as mitigation strategies on the device level could potentially be employed.<sup>81–83</sup> Consequently, the catalyst utilized in an H<sub>2</sub>O<sub>2</sub> electrolyser is subjected to analogous potential-driven degradation mechanisms as mentioned earlier for H<sub>2</sub>O<sub>2</sub>-FC. If the applied potential surpasses the reduction potential of the M<sup>x+</sup>/M redox couple, it is likely to induce a change in the valence state of surface atoms at sufficiently high overpotentials.<sup>84–86</sup> These conditions can trigger structural reconstruction of the catalyst based on metals in a positive oxidation state, such as oxides or SACs, potentially leading to transformations of active sites, including the reduction to its metallic state followed by dissolution or agglomeration/cluster formation.<sup>29,87</sup>

A vital factor is the presence of H<sub>2</sub>O<sub>2</sub> in close vicinity to the catalyst material as it may act as a degradation agent itself. H<sub>2</sub>O<sub>2</sub> is known as an oxidising agent for organic matter and is used as bleaching agent, disinfectant, and antiseptic.<sup>5,88,89</sup> The oxidative nature of H<sub>2</sub>O<sub>2</sub> ( $E_{\text{H}_2\text{O}_2/\text{H}_2\text{O}}^0 = 1.76 \text{ V}_{\text{SHE}}$ ) challenges the longevity of electrocatalysts employed in its production.<sup>90</sup> Of particular concern is the potential formation of stronger or more reactive oxygen species (ROS) during H<sub>2</sub>O<sub>2</sub> decomposition, such as hydroxyl ( $\bullet\text{OH}$ ,  $E_{\text{OH}/\text{H}_2\text{O}}^0 = 2.80 \text{ V}_{\text{SHE}}$ ) and hydroperoxyl ( $\bullet\text{OOH}$ ,  $E_{\text{OOH}/\text{H}_2\text{O}_2}^0 = 1.44 \text{ V}_{\text{SHE}}$ ) radicals in the presence of UV radiation or dissolved transition-metal ions.<sup>90–92</sup> Effectively

addressing the impact of ROS is imperative for enhancing the durability and sustained performance of electrocatalysts employed in the H<sub>2</sub>O<sub>2</sub> production. In the previous section, it became clear that the unifying element in nearly all described catalyst materials lies in the utilization of carbon, either directly or as a supporting material, to achieve a high dispersion of the active catalyst. The generated ROS, especially the hydroxyl radical, renowned as the second strongest oxidizing agent after fluorine, can rapidly induce changes in the carbon matrix such as bond breakage ultimately leading to transformation into CO or CO<sub>2</sub>.<sup>90,93–96</sup>

For example,  $\bullet\text{OH}$  can be generated by the gradual homolysis of H<sub>2</sub>O<sub>2</sub>. A reported rate constant of  $1.2 \times 10^{-7} \text{ s}^{-1}$  at room temperature and low pH emphasizes the controlled formation of these radicals.<sup>97</sup> However,  $\bullet\text{OH}$  is also chemically generated much faster through the classical Fenton reaction (reaction rate of  $ca. 60 \text{ M}^{-1} \text{ s}^{-1}$ ),<sup>90,98</sup> involving a mixture of diluted H<sub>2</sub>O<sub>2</sub> solution and a Fe<sup>2+</sup> species in acidic media (eqn (1)), following rather a heterolytic than a homolytic pathway.

The efficient homogeneous generation of hydroxyl radicals can be attributed to the high electron transfer cycle rate of the Fe<sup>3+</sup>/Fe<sup>2+</sup> redox couple, particularly in solutions with a pH around 3.<sup>90</sup> Even small amounts of Fe<sup>2+</sup> are sufficient due to their ability to be regenerated from the homogeneous Fenton-like reaction (eqn (2)).<sup>99</sup> The Fenton-like reaction is expected to be approximately four orders of magnitude slower than the classical Fenton reaction, eqn (1) ( $ca. 2 \times 10^{-3} \text{ M}^{-1} \text{ s}^{-1}$ ).<sup>98</sup> However, the consumed Fe<sup>2+</sup> can be regenerated more rapidly ( $ca. 2 \times 10^6 \text{ M}^{-1} \text{ s}^{-1}$ ) through the reduction of Fe<sup>3+</sup> with  $\bullet\text{OOH}$  (eqn (3)).<sup>98</sup> Furthermore, the electrochemical regeneration of Fe<sup>2+</sup> at the cathode is possible (eqn (4)).<sup>100</sup>



Numerous studies especially in the context of advanced oxidation processes and as well as in durability of low temperature PEM-FC-4e<sup>-</sup> on various heterogeneous catalysts have explored their effectiveness in the Fenton and Fenton-like reaction (when the reaction is based on Fe<sup>3+</sup> or on another reactant). These reactions involve diverse metals and are not limited to Fe as classical Fenton and Fenton-like catalysts including metals such as Cu, Mn, Ce, Cr, Co, Ru, Pd, Ag, and Au.<sup>97,99,101–106</sup> In principle, several metals can generate radicals from H<sub>2</sub>O<sub>2</sub> heterogeneously or through partly homogeneous Fenton-like chemistry. The unifying element is the prevalence of varying oxidation states. These oxidation states must remain stable over a wide pH range to prevent catalyst loss through leaching, and the metallic species should resist hydration forces and remain insoluble.

Despite the fact that most of these metals are less effective in Fenton and Fenton-like reactions than homogeneous Fe<sup>2+</sup>, these metals facilitate ROS production, typically through





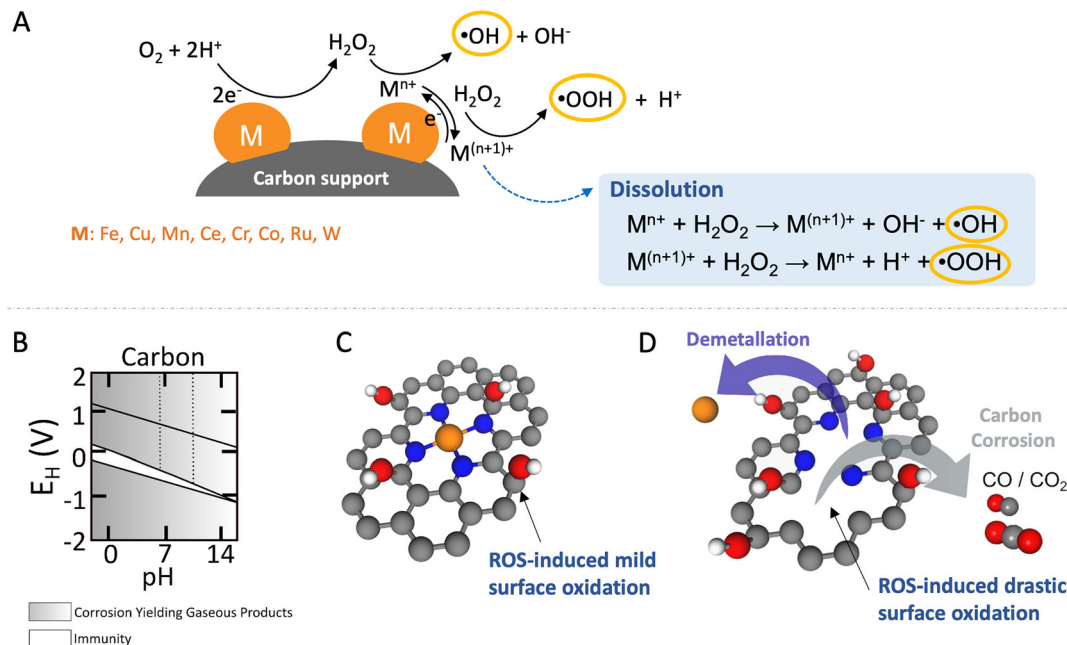


**Fig. 3** Schematic illustration depicting homogeneous and heterogeneous Fenton and Fenton-like reactions, showcasing their influence on carbon-based catalysts during the ORR. (A) Depiction of homogeneous and heterogeneous Fenton and Fenton-like reactions. (B) Potential–pH diagram for carbon in aqueous solutions. (C) Mild and reversible oxidation of carbon supports. (D) Irreversible oxidation or corrosion of carbon supports along with the demetallation. Color coding for the components: metal active sites, orange; C, gray; O, red; N, blue; and H, white. Panel B is adapted with permission from ref. 111 Copyright 1973 Springer Nature.

electron-transfer steps that alter the oxidation state of the metal, leading to the generation of  $\bullet OH$  and  $\bullet OOH$  as schematically shown in Fig. 3(A).<sup>107</sup> Conversely, metals resistant to oxidation state changes, like Al, Ga, In, Zr, and Ti, also play a role in generating ROS from  $H_2O_2$  through a metal hydroperoxo species,  $[M]-OOH$ , without direct electron transfer involvement.<sup>107</sup> Additionally, ROS production can occur from the reaction of adsorbed protons with  $H_2O_2$  on noble metals such as Ag, Pt, Rh, or Pd.<sup>108–110</sup> Generally, all these processes of ROS generation from  $H_2O_2$  exhibit slower rates compared to the homogeneous Fenton reaction. This difference is attributed to the additional mass transport barrier for  $H_2O_2$  to access the solid-phase catalyst for Fenton and Fenton-like reactions.

In heterogeneous Fenton or Fenton-like catalysis, reducing particle size is expected to enhance the process efficiency. This is because a smaller particle size translates to a larger active surface area. This increased surface area provides more sites for the adsorption of reactants (hydrogen peroxide and target pollutants) and the generation of hydroxyl radicals, ultimately leading to faster reaction rates and potentially improved degradation of contaminants. Furthermore, SACs typically exhibit greater atom utilisation than NPs, they can show higher mass normalised Fenton or Fenton-like activity, as well as catalytic activity comparable or superior to homogeneous catalysts.<sup>112,113</sup>

The choice of support material significantly influences the stability and longevity of the catalyst as secondary degradation effects, such as nanoparticle agglomeration/coalescence or detachment are mitigated.<sup>114–118</sup> Carbon-based materials,

for instance, primarily degrade due to carbon oxidation at sufficiently high potentials.<sup>50,119</sup> Thermodynamically, carbon exhibits a small immunity region in aqueous solutions as illustrated in Fig. 3(B), and can oxidize to  $CO_2$  and  $CO$  at  $E_{C/CO_2}^0 = 0.21 V_{SHE}$  and  $E_{C/CO}^0 = 0.52 V_{SHE}$ , respectively. These values significantly differ from  $E_{H_2O_2/H_2O}^0$ ,  $E_{\bullet OH/H_2O}^0$ , or  $E_{\bullet OOH/H_2O_2}^0$ , thereby facilitating the thermodynamic oxidation of carbon materials by hydrogen peroxide.<sup>120</sup>

Kumar *et al.* demonstrated that subjecting a non-noble based catalyst to an electrochemical accelerated stress test (AST) in oxygen-containing electrolyte leads to a notable loss of iron within the  $FeN_x$  sites of the catalyst. This loss is caused by the corrosion of the catalyst's carbon, facilitated either by  $H_2O_2$  or radical species derived from  $H_2O_2$ .<sup>121</sup> The same holds true for noble metal based catalysts. The presence of oxygen notably affects the degradation of Pt/C in the potential range of 0.05 to 0.5  $V_{RHE}$ . In this range, the two-electron ORR pathway generates  $H_2O_2$ -derived radical species which, in turn, inflicts damage on the carbon supports.<sup>122</sup> Chemical oxidative stress can be intensified in Fe- and Co-based non-noble metal catalysts supported on carbon-based supports, as the chemical disproportionation of  $H_2O_2$  on these catalysts generates a significant amount of ROS.<sup>50,123</sup> It has been demonstrated that the Fe–N–C structure undergoes stronger degradation, along with a loss in ORR activity, when subjected to load cycling and start/stop testing in RDE and PEMFC,<sup>124</sup> and potential hold in PEMFC<sup>125</sup> in  $O_2$ - vs. Ar-saturated acidic electrolyte. In addition, after enduring 10 000 potential cycles from 0.6 to 1.0  $V_{RHE}$  and



100 hours hold at a potential of 0.7 V<sub>RHE</sub> in O<sub>2</sub>-purged electrolyte, Co–N–C catalysts exhibited superior durability compared to Fe–N–C.<sup>126</sup> The enhanced stability is attributed to the lower reactivity of Co ions in Fenton-like reactions that generate radicals from H<sub>2</sub>O<sub>2</sub>. Complementing this finding, Laconti *et al.* suggested a hierarchy for the rate of chemical degradation by certain contaminants: Fe<sup>2+</sup> impacts degradation rate the most, followed by Cu<sup>2+</sup>, TiO<sup>2+</sup>, Co<sup>2+</sup>, Pt<sup>2+</sup>, and Ni<sup>2+</sup>.<sup>127</sup> The potential involvement of H<sub>2</sub>O<sub>2</sub> and ROS species in catalytic processes was highlighted by Lefèvre *et al.*<sup>128</sup> They observed that exposing Fe-based catalysts to a solution of 5 vol% H<sub>2</sub>O<sub>2</sub> in 1 M H<sub>2</sub>SO<sub>4</sub> solution for 5 hours – mimicking amounts of produced H<sub>2</sub>O<sub>2</sub> similar to those found in ORR with a 2 wt% Pt/C catalyst led to a significant ORR activity loss of approximately 180 mV. This loss in catalytic efficiency was linearly correlated with the Fe loss within the catalyst induced by H<sub>2</sub>O<sub>2</sub>.

The efficiency of the Fenton reaction is influenced by temperature, pH, as well as H<sub>2</sub>O<sub>2</sub>, and iron concentration, with temperature being the most impactful, followed by Fe<sup>2+</sup> and H<sub>2</sub>O<sub>2</sub> concentration.<sup>127,129</sup> Higher temperatures tend to increase the rate of the Fenton reaction, but they also increase the disproportionation of H<sub>2</sub>O<sub>2</sub> into O<sub>2</sub> and H<sub>2</sub>O.<sup>130</sup>

In the absence of iron, •OH is produced by homolytic dissociation of H<sub>2</sub>O<sub>2</sub> (H<sub>2</sub>O<sub>2</sub> → 2 •OH) on Pt catalyst. At an H<sub>2</sub>O<sub>2</sub> concentration of 1 M, Gubler *et al.* reported that 45% of •OH are created *via* •OOH formation (•OH + H<sub>2</sub>O<sub>2</sub> → •OOH + H<sub>2</sub>O, •OOH + H<sub>2</sub>O<sub>2</sub> → •OH + H<sub>2</sub>O + O<sub>2</sub>).<sup>101</sup> Without Fe-ion impurities, •OOH primarily dismutates to H<sub>2</sub>O<sub>2</sub> and O<sub>2</sub>, yet there remains a possibility for it to contribute to chemical oxidation of *e.g.* carbon.<sup>122</sup> However, with typical Fe-ion impurities found in fuel cell membranes (around 1 ppm) and concentrations up to several millimolar H<sub>2</sub>O<sub>2</sub>, Fe ions catalyse •OH generation. The rate of •OH formation *via* the Fenton reaction is eight times higher than by homolysis, becoming the predominant source when Fe impurity levels exceed 40 ppm (1.1 mM).<sup>131</sup>

Carbon nanostructures exhibit varying levels and types of metallic impurities, which depend on the specific preparation methods used.<sup>132</sup> For instance, analyses using ICP-MS reveal that bare graphite typically contains about 4 ppm of Fe. In graphene oxide, the metallic impurities were found to be different, comprising 3800 ppm of Mn, 120 ppm of Cu, 53 ppm of Fe, and 4 ppm of Ni. In a similar vein, carbon nanotubes display varied impurity profiles, with concentrations of 1200 ppm for Ni, 90 ppm for Fe, 11 ppm for Mn, and 3 ppm for Cu.<sup>133</sup> Consequently, the influence of Fe and other metal impurities on the conversion of H<sub>2</sub>O<sub>2</sub> into ROS in ostensibly metal-free catalysts is a critical consideration for carbon corrosion that cannot be overlooked.

The corrosion rate of carbon is notably affected by material properties, including surface area, porosity, degree of graphitisation, and heteroatom doping, all of which play pivotal roles in determining the overall durability of the catalyst system.<sup>134–136</sup> ROS, generated through the decomposition of H<sub>2</sub>O<sub>2</sub>, readily interacts with unsaturated aliphatic or aromatic carbon compounds mainly at the edges, leading to the formation of oxygen-containing functional groups like –COOH, and –COH on the

surface, as illustrated in Fig. 3(C). Ultimately, this process, detailed in Fig. 3(D), facilitates the conversion of volatile carbon corrosion products such as CO or CO<sub>2</sub> and leads to metal dissolution and/or detachment (demetallation).<sup>121,123,128</sup> In more applied H<sub>2</sub>O<sub>2</sub> production devices using MEA or GDE (or both) configurations, the generation of hydrophilic groups by oxidation during operation causes flooding of the catalyst layer leading to mass transport related losses.<sup>137</sup> In the case of catalysts containing active centers or organic ligands, such as catalysts based on organic molecules, organo-metallic complexes, and SACs, the impact on catalytic activity and selectivity can be even more pronounced.<sup>125</sup>

The intrinsic non-polarity of carbon makes it challenging to exhibit robust metal-support interactions without having anchoring functional groups present.<sup>138</sup> The incorporation of oxygen functional groups onto carbon surfaces not only augments the number of anchoring sites for deposited particles/clusters/single atoms but also improves the catalytic activity and selectivity. The presence of carboxyl, carbonyl, and quinone functional groups on the carbon surface plays a vital role in enhancing the Fenton reaction. These groups expedite the conversion of Fe<sup>3+</sup> to Fe<sup>2+</sup>, which is a pivotal step in the catalytic iron cycle. This conversion is particularly significant as it constitutes the rate-limiting step, profoundly influencing the efficiency of the reaction.<sup>103</sup> Consequently, they can promote carbon oxidation and metal detachment/dissolution by increasing the ROS production rate. Resistance to carbon corrosion can be notably improved through graphitisation. Graphitised carbon supports exhibit remarkable long-term stability compared to disordered amorphous carbon supports.<sup>139,140</sup> Enhancing ORR activity can be achieved by incorporating heteroatoms like nitrogen into their structure, which increases the negative charge density on adjacent carbon atoms. H<sub>2</sub>O<sub>2</sub> and ROS, generated *in situ* at FeN<sub>x</sub> sites during ORR, induce mild surface oxidation, as previously reported in *ex situ* treatments of Fe–N–C with H<sub>2</sub>O<sub>2</sub>.<sup>141</sup> However, they also trigger irreversible carbon corrosion. This corrosion forms volatile CO and CO<sub>2</sub>, creating new pores and increasing carbon surface area, while simultaneously disintegrating metal–N sites, resulting in demetallation and a decrease in catalytic activity.<sup>124</sup>

The decay of active sites and the oxidation of the carbon matrix are driven by a combination of electrochemical and chemical oxidation processes, with H<sub>2</sub>O<sub>2</sub>/ROS notably accelerating the chemical oxidation. Considering that H<sub>2</sub>O<sub>2</sub> is the predominant product in ORR-2e<sup>−</sup>, closely examining its release rate during durability and stability tests becomes crucial. Simultaneously, standardised protocols play a crucial role in facilitating consistent comparisons of catalytic performance among various research groups.

## 4. Key considerations in unravelling catalyst degradation

While some degradation assessment protocols exist for specific electrochemical reactions, such as ORR-4e<sup>−</sup>,<sup>142–144</sup> there is an



absence of benchmarked protocols for the ORR- $2e^-$ . Accelerated stress tests can be utilized to induce and study catalyst (and cell) aging processes, as well as evaluate failure modes under real-world conditions. In the following discussion, our focus will be solely on catalyst-related aspects, excluding other potential failure modes. Establishing suitable degradation protocols and reliable measurement configurations at an early stage of electrocatalyst development is a fundamental task in this context. In light of the considerations mentioned earlier, a key objective is to design AST protocols capable of simulating specific scenarios that mirror the most challenging conditions imposed on the catalyst material. This includes scenarios such as start-stop cycling, continuous operation under  $H_2O_2$  production, and extended contact with  $H_2O_2$  at OCP.

For PEM-FCs, AST protocols are capable of simulating the degradation of the catalysts at start-stop conditions. Typically, the catalysts are subjected to square wave voltammetry, using an operation potential, *e.g.*  $0.6 V_{RHE}$  and OCP, usually  $\leq 1.0 V_{RHE}$  for Pt and Pd-based catalysts. In Fig. 4(A), we exemplify a possible potential square wave-based AST for ORR- $2e^-$  catalysts, where the upper and lower potential limits are the OCP and the voltage recorded when forcing a certain  $H_2O_2$ -generation current density ( $J$ ), respectively. Both, upper and lower potentials depend strongly on the catalysts employed and have to be measured for each catalyst system.

As  $H_2O_2$  itself can inflict damage to the catalyst, evaluating its stability involves testing under practical electrolysis operating

conditions and realistic  $H_2O_2$  concentration in direct contact with the catalyst. Rather than relying solely on the applied potential, chronopotentiometric methods (Fig. 4(B)) allow quantitative insights into the potential contribution of generated  $H_2O_2$  to the degradation process. When operated at high current densities of hundreds of  $mA\ cm^{-2}$ , the applied potential becomes more and more negative creating a reductive environment. These reductive conditions, particularly relevant for catalysts composed of metals with positive oxidation states such as in oxides or single-atom catalysts, have the potential to induce structural changes, potentially leading to oxidation state changes, as discussed in Section 3.

During early-stage catalytic testing, conventional laboratory-scale electrochemical setups, such as rotating ring-disk electrode setups (RRDE) are commonly employed. However, limitations in  $O_2$  mass transport may hinder the attainment of practical  $H_2O_2$ -generation current densities, thereby preventing continuous exposure of the catalyst to realistic  $H_2O_2$  concentrations. Acknowledging this challenge, we propose a supplementary protocol that aligns with the previously discussed protocols. This method involves conducting ASTs in an electrolyte solution containing  $H_2O_2$ , as illustrated in Fig. 4(C). Here, the catalyst is directly immersed in an  $H_2O_2$ -containing electrolyte solution such as *e.g.*, 10 mM  $H_2O_2$  for an extended duration. Thereby, a comparative analysis of chemical decomposition rates can be obtained. By conducting these three protocols, catalysts can be evaluated for their stability and compared. Further adaptation of these protocols

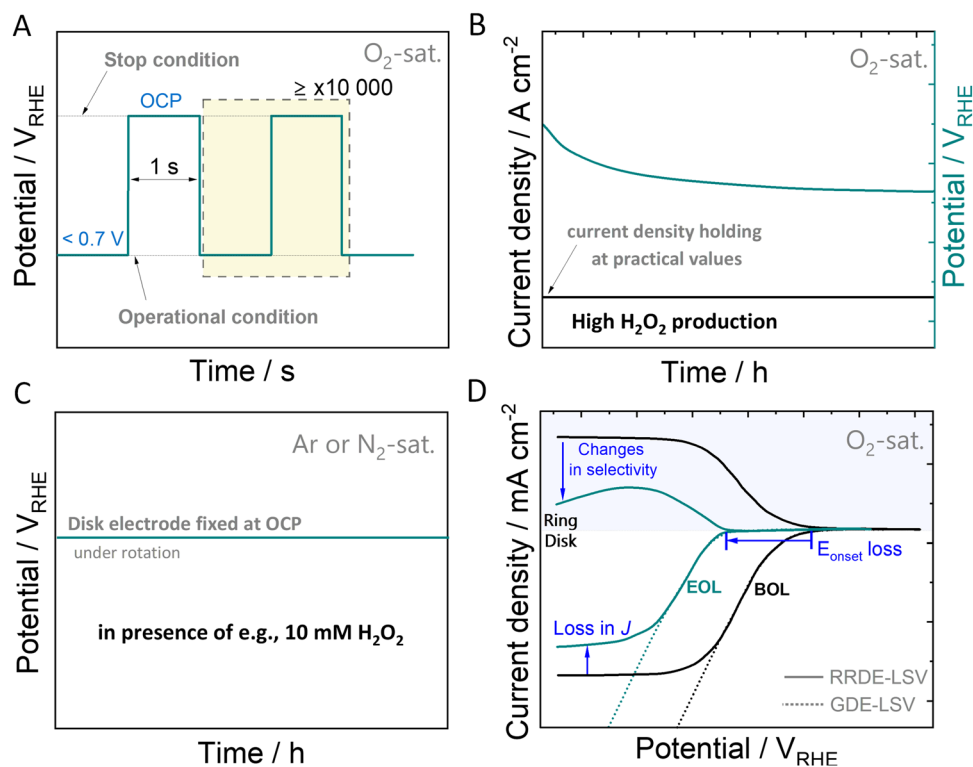


Fig. 4 Schematic representation of the process for standardising degradation assessment protocols. Illustration of accelerated stress test protocol profiles simulating: (A) start-stop regimes, (B) practical electrolysis operating conditions, and (C) influence of the contact of  $H_2O_2$  with the catalyst. Schematic responses for (D) RRDE- and GDE-LSV curves for ORR study.



will have to follow, depending on the catalyst used and the involved degradation mechanism of the specific catalyst material. The disparity in catalytic performance observed in polarisation curves, such as linear sweep voltammetry (LSV) curves, taken at the initiation and the end of the protocol, referred to as beginning of life (BOL) and end of life (EOL), provides valuable insights into the degradation induced by the accelerated stress test (Fig. 4(D)). This comparison aids in understanding changes in terms of ORR activity and selectivity, facilitating the evaluation of the catalyst's stability. To monitor variations in parameters such as onset potential, faradaic efficiency, mass activity, or losses of the electrochemical surface area should be considered.

## 5. Challenges and limitations

In the supporting information, we provide a comprehensive discussion of the obstacles and constraints associated with the performance of the catalyst in order to successfully implement the electrochemical  $\text{H}_2\text{O}_2$  production. The efficiency of catalysts plays a crucial role in the cost-effectiveness of electrochemical technologies, underscoring the importance of enhancing catalyst efficiency and durability for substantial cost reduction.

For practical applications, it is crucial that electrodes maintain high stability for  $\text{H}_2\text{O}_2$  production across long-term operations and under varying conditions. Supporting substrates that hold nanoparticles or single atoms may chemically or physically degrade, significantly impacting performance. Currently, carbon materials are the preferred support for ORR catalysts because of their low cost and beneficial properties such as conductivity, variability in changing pore size and pore volume, chemical resistance and non-toxicity. However, carbon corrosion, which occurs at high electrode potentials and is exacerbated by ROS from  $\text{H}_2\text{O}_2$ , can lead to the detachment/agglomeration of metal particles/atoms from the support and subsequent performance degradation, as exemplified in Section 3. Arguably, future research should aim to enhance the stability of carbon-supported SACs in acidic conditions, possibly by modifying these supports with functional groups that may act as anchor point for the active metal. For instance, Chen *et al.* observed that thiolated carbon supports (Pt/SH-CNTs) significantly enhance the resistance against Pt dissolution at high potentials.<sup>145</sup> More recently, Wang *et al.* demonstrated that graphitic N-doped  $\text{CoN}_4\text{C}$  ( $\text{CoN}_4\text{C-N}$ ) catalysts achieve 82% Faraday efficiency for  $\text{H}_2\text{O}_2$  in a flow cell, delivering a yield of  $0.096 \text{ mmol cm}^{-2} \text{ h}^{-1}$  over 200 h at  $0.358 \text{ V}_{\text{RHE}}$ , highlighting the important role of graphitic nitrogen.<sup>37</sup>

To our knowledge, little research has focused on catalyst stability in the context of  $\text{H}_2\text{O}_2$  electrogeneration. We argue that for industrial applications, a thorough understanding of catalytic performance and degradation is crucial. In practical scenarios, high concentrations of  $\text{H}_2\text{O}_2$  accumulating at the solid/liquid interface may decompose, leading to accelerated

corrosion of the electrode and degradation of the catalyst.<sup>146</sup> This decomposition can intensify the  $\text{H}_2\text{O}_2$ -induced oxidation process, causing the catalyst to detach from the support, agglomerate or dissolve into the electrolyte.

## 6. Summary and outlook

In summary, we have shown the crucial significance of catalyst stability in the electrocatalytic production of  $\text{H}_2\text{O}_2$ , emphasising essential considerations for designing and testing catalysts tailored to this application. Our analysis identifies several primary factors contributing to catalyst degradation, thereby leading to diminished  $\text{H}_2\text{O}_2$  electrogeneration efficiency in devices. These factors include low pH values, potential-driven degradation, and the susceptibility of catalyst degradation induced by reactive oxygen species. Notably,  $\text{H}_2\text{O}_2$  itself may act as a degradation agent. The oxidative nature of  $\text{H}_2\text{O}_2$ , coupled with the rapid kinetics of generated radicals, significantly impacts the longevity of electrocatalysts utilized in its production. Given that carbon serves as a unifying element in nearly all described ORR- $2e^-$  catalyst materials, whether directly or as a supporting material, it is imperative to effectively address the impact of ROS for enhancing the durability and sustained performance of electrocatalysts used in  $\text{H}_2\text{O}_2$  production. Furthermore, considering the current absence of benchmarked AST protocols for ORR- $2e^-$ , and the need for the development and adoption of comprehensive standardised testing methodologies, we have made a first attempt to present three AST protocols capable of simulating specific scenarios that mirror the most challenging conditions imposed on the catalyst material during  $\text{H}_2\text{O}_2$  production. By bridging gaps in our understanding of catalyst behaviour under realistic conditions, we can pave the way for the development of robust catalysts capable of withstanding the challenges posed by  $\text{H}_2\text{O}_2$  electrogeneration.

## Author contributions

The manuscript was written through the contributions of all authors. All authors have approved the final version of the manuscript.

## Conflicts of interest

The authors declare no competing financial interest.

## Acknowledgements

J. S. C. and M. L. are grateful to the Federal Ministry of Education and Research (BMBF) for the financial support received in the framework of NanoMatFutur (SynKat, FK: 03XP0265). G. V. F., J. C. L., and M. R. V. L. are grateful for the financial support received from the São Paulo Research Foundation (FAPESP – grants #2017/10118-0, #2023/04230-2, #2021/12053-8, #2019/04421-7, and # 2021/14194-8) and





Brazilian National Council for Scientific and Technological Development (CNPq – grant #303943/2021-1). M. L. gratefully acknowledges funding within the framework of Fe-Upgraded from the “Deutsche Forschungsgemeinschaft” (DFG, German Research Foundation) – Project-ID 443703006 – CRC 1487.

## References

- S. Möhle, M. Zirbes, E. Rodrigo, T. Gieshoff, A. Wiebe and S. R. Waldvogel, *Angew. Chem., Int. Ed.*, 2018, **57**, 6018–6041.
- R. Xia, S. Overa and F. Jiao, *JACS Au*, 2022, **2**, 1054–1070.
- N. Dyantyi, J. C. Calderón Gómez, L. Mekuto, P. Bujlo and G. Patrick, *Electrocatalysts: Selectivity and utilization*, INC, 2021.
- S. Siahrostami, A. Verdaguier-Casadevall, M. Karamad, D. Deiana, P. Malacrida, B. Wickman, M. Escudero-Escribano, E. A. Paoli, R. Frydendal, T. W. Hansen, I. Chorkendorff, I. E. L. Stephens and J. Rossmeisl, *Nat. Mater.*, 2013, **12**, 1137–1143.
- G. V. Fortunato, E. Pizzutilo, I. Katsounaros, D. Göhl, R. J. Lewis, K. J. J. Mayrhofer, G. J. Hutchings, S. J. Freakley and M. Ledendecker, *Nat. Commun.*, 2022, **13**, 1–7.
- E. Kolle-Görgen, G. Fortunato and M. Ledendecker, *Chem. Mater.*, 2022, **34**, 10223–10236.
- A. Verdaguier-Casadevall, D. Deiana, M. Karamad, S. Siahrostami, P. Malacrida, T. W. Hansen, J. Rossmeisl, I. Chorkendorff and I. E. L. Stephens, *Nano Lett.*, 2014, **14**, 1603–1608.
- J. S. Jirkovsk, I. Panas, E. Ahlberg, M. Halasa, S. Romani and D. J. Schi, *J. Am. Chem. Soc.*, 2011, **14**, 19432–19441.
- M. Inaba, H. Yamada, J. Tokunaga and A. Tasaka, *Electrochem. Solid-State Lett.*, 2004, **7**, 474–476.
- E. Fabbri, S. Taylor, A. Rabis, P. Levecque, O. Conrad, R. Kötz and T. J. Schmidt, *ChemCatChem*, 2014, **6**, 1410–1418.
- E. Antolini, *Appl. Catal., B*, 2016, **181**, 298–313.
- M. Nesselberger, M. Roefzaad, R. Fayçal Hamou, P. Ulrich Biedermann, F. F. Schweinberger, S. Kunz, K. Schloegl, G. K. H. Wiberg, S. Ashton, U. Heiz, K. J. J. Mayrhofer and M. Arenz, *Nat. Mater.*, 2013, **12**, 919–924.
- G. V. Fortunato, E. Pizzutilo, A. M. Mingers, O. Kasian, S. Cherevko, E. S. F. Cardoso, K. J. J. Mayrhofer, G. Maia and M. Ledendecker, *J. Phys. Chem. C*, 2018, **122**, 15878–15885.
- C. H. Choi, H. C. Kwon, S. Yook, H. Shin, H. Kim and M. Choi, *J. Phys. Chem. C*, 2014, **118**, 30063–30070.
- A. Ohma, K. Fushinobu and K. Okazaki, *Electrochim. Acta*, 2010, **55**, 8829–8838.
- J. Chlistunoff and B. Pivovar, *ECS Meet. Abstr.*, 2007, **MA2007-02**, 506.
- S. J. Freakley, Q. He, J. H. Harrhy, L. Lu, D. A. Crole, D. J. Morgan, E. N. Ntainjua, J. K. Edwards, A. F. Carley, A. Y. Borisevich, C. J. Kiely and G. J. Hutchings, *Science*, 2016, **351**, 965–968.
- D. He, L. Zhong, S. Gan, J. Xie, W. Wang, Z. Liu, W. Guo, X. Yang and L. Niu, *Electrochim. Acta*, 2021, **371**, 137721.
- S. Yang, J. Kim, Y. J. Tak, A. Soon and H. Lee, *Angew. Chem., Int. Ed.*, 2016, **55**, 2058–2062.
- S. Yang, Y. J. Tak, J. Kim, A. Soon and H. Lee, *ACS Catal.*, 2017, **7**, 1301–1307.
- C. H. Choi, M. Kim, H. C. Kwon, S. J. Cho, S. Yun, H. T. Kim, K. J. J. Mayrhofer, H. Kim and M. Choi, *Nat. Commun.*, 2016, **7**, 10922.
- M. Ledendecker, E. Pizzutilo, G. Malta, G. V. Fortunato, K. J. J. Mayrhofer, G. J. Hutchings and S. J. Freakley, *ACS Catal.*, 2020, **10**, 5928–5938.
- Q. Chang, P. Zhang, A. H. B. Mostaghimi, X. Zhao, S. R. Denny, J. H. Lee, H. Gao, Y. Zhang, H. L. Xin, S. Siahrostami, J. G. Chen and Z. Chen, *Nat. Commun.*, 2020, **11**, 1–9.
- J. S. Choi, S. Yoo, E. S. Koh, R. Aymerich-Armengol, C. Scheu, G. V. Fortunato, M. R. V. Lanza, Y. J. Hwang and M. Ledendecker, *Adv. Mater. Interfaces*, 2023, **10**, 1–7.
- X. Yang, A. Wang, B. Qiao, J. Li, J. Liu and T. Zhang, *Acc. Chem. Res.*, 2013, **46**, 1740–1748.
- J. C. Meier, C. Galeano, I. Katsounaros, J. Witte, H. J. Bongard, A. A. Topalov, C. Baldizzone, S. Mezzavilla, F. Schüth and K. J. J. Mayrhofer, *Beilstein J. Nanotechnol.*, 2014, **5**, 44–67.
- A. Wang, J. Li and T. Zhang, *Nat. Rev. Chem.*, 2018, **2**, 65–81.
- Y. Nie, L. Li and Z. Wei, *Chem. Soc. Rev.*, 2015, **44**, 2168–2201.
- F. D. Speck, M. T. Y. Paul, F. Ruiz-Zepeda, M. Gatalo, H. Kim, H. C. Kwon, K. J. J. Mayrhofer, M. Choi, C. H. Choi, N. Hodnik and S. Cherevko, *J. Am. Chem. Soc.*, 2020, **142**, 15496–15504.
- H. E. Kim, I. H. Lee, J. Cho, S. Shin, H. C. Ham, J. Y. Kim and H. Lee, *ChemElectroChem*, 2019, **6**, 4757–4764.
- J. Xi, S. Yang, L. Silvioli, S. Cao, P. Liu, Q. Chen, Y. Zhao, H. Sun, J. N. Hansen, J. P. B. Haraldsted, J. Kibsgaard, J. Rossmeisl, S. Bals, S. Wang and I. Chorkendorff, *J. Catal.*, 2021, **393**, 313–323.
- M. Campos, W. Siriwatcharapiboon, R. J. Potter and S. L. Horswell, *Catal. Today*, 2013, **202**, 135–143.
- Y. Sun, L. Silvioli, N. R. Sahaie, W. Ju, J. Li, A. Zitolo, S. Li, A. Bagger, L. Arnarson, X. Wang, T. Moeller, D. Bernsmeier, J. Rossmeisl, F. Jaouen and P. Strasser, *J. Am. Chem. Soc.*, 2019, **141**, 12372–12381.
- J. Gao, H. bin Yang, X. Huang, S. F. Hung, W. Cai, C. Jia, S. Miao, H. M. Chen, X. Yang, Y. Huang, T. Zhang and B. Liu, *Chem*, 2020, **6**, 658–674.
- Z. Jiajun, F. Cehuang, Y. Ke, L. Zheng, J. Fangling, S. Shuiyun, Z. Xiaoran, M. Lu, S. Zulipiya, W. Xiaoming, Z. Junliang and J. Kun, *Nat. Commun.*, 2022, **13**, 1–10.
- F. Wu, C. Pan, C. T. He, Y. Han, W. Ma, H. Wei, W. Ji, W. Chen, J. Mao, P. Yu, D. Wang, L. Mao and Y. Li, *J. Am. Chem. Soc.*, 2020, **142**, 16861–16867.
- W. Wang, Y. Hu, P. Li, Y. Liu and S. Chen, *ACS Catal.*, 2024, **14**, 5961–5971.
- S. Chen, T. Luo, X. Li, K. Chen, J. Fu, K. Liu, C. Cai, Q. Wang, H. Li, Y. Chen, C. Ma, L. Zhu, Y. R. Lu, T. S. Chan,



- M. Zhu, E. Cortés and M. Liu, *J. Am. Chem. Soc.*, 2022, **144**, 14505–14516.
- 39 H. Huang, M. Sun, S. Li, S. Zhang, Y. Lee, Z. Li, J. Fang, C. Chen, Y.-X. Zhang, Y. Wu, Y. Che, S. Qian, W. Zhu, C. Tang, Z. Zhuang, L. Zhang and Z. Niu, *J. Am. Chem. Soc.*, 2024, **146**, 9434–9443.
- 40 T. P. Fellingner, F. Hasché, P. Strasser and M. Antonietti, *J. Am. Chem. Soc.*, 2012, **134**, 4072–4075.
- 41 S. K. Singh, K. Takeyasu and J. Nakamura, *Adv. Mater.*, 2019, **31**, 1–17.
- 42 G. F. Han, F. Li, W. Zou, M. Karamad, J. P. Jeon, S. W. Kim, S. J. Kim, Y. Bu, Z. Fu, Y. Lu, S. Siahrostami and J. B. Baek, *Nat. Commun.*, 2020, **11**, 1–9.
- 43 A. Wang, A. Bonakdarpour, D. P. Wilkinson and E. Gyenge, *Electrochim. Acta*, 2012, **66**, 222–229.
- 44 R. B. Valim, R. M. Reis, P. S. Castro, A. S. Lima, R. S. Rocha, M. Bertotti and M. R. V. Lanza, *Carbon N. Y.*, 2013, **61**, 236–244.
- 45 P. Cui, L. Zhao, Y. Long, L. Dai and C. Hu, *Angew. Chem., Int. Ed.*, 2023, **62**, e202218269.
- 46 K. Mamtani and U. S. Ozkan, *Catal. Lett.*, 2015, **145**, 436–450.
- 47 Y. Sun, I. Sinev, W. Ju, A. Bergmann, S. Dresp, S. Köhl, C. Spöri, H. Schmies, H. Wang, D. Bernsmeier, B. Paul, R. Schmack, R. Kraehnert, B. Roldan Cuenya and P. Strasser, *ACS Catal.*, 2018, **8**, 2844–2856.
- 48 Z. H. Sun, X. Zhang, X. D. Yang, W. N. Shi, Y. Q. Huang, Y. L. Men, J. Yang and Z. Y. Zhou, *Chem. Commun.*, 2022, **58**, 8998–9001.
- 49 H. Singh, S. Zhuang, B. Ingis, B. B. Nunna and E. S. Lee, *Carbon N. Y.*, 2019, **151**, 160–174.
- 50 D. Banham, S. Ye, K. Pei, J. I. Ozaki, T. Kishimoto and Y. Imashiro, *J. Power Sources*, 2015, **285**, 334–348.
- 51 J. Zhang, Y. Yuan, L. Gao, G. Zeng, M. Li and H. Huang, *Adv. Mater.*, 2021, **33**, 1–23.
- 52 Z. Chen, D. Higgins, A. Yu, L. Zhang and J. Zhang, *Energy Environ. Sci.*, 2011, **4**, 3167–3192.
- 53 C. H. Choi, C. Baldizzone, J. P. Grote, A. K. Schuppert, F. Jaouen and K. J. J. Mayrhofer, *Angew. Chem., Int. Ed.*, 2015, **54**, 12753–12757.
- 54 M. Sun, S. Gong, Y. X. Zhang and Z. Niu, *J. Energy Chem.*, 2022, **67**, 250–254.
- 55 U. I. Kramm, L. Ni and S. Wagner, *Adv. Mater.*, 2019, **31**, 1–11.
- 56 S. J. Ashton and M. Arenz, *J. Power Sources*, 2012, **217**, 392–399.
- 57 Y. Yang, Y. Xiong, R. Zeng, X. Lu, M. Krumov, X. Huang, W. Xu, H. Wang, F. J. DiSalvo, J. D. Brock, D. A. Muller and H. D. Abruña, *ACS Catal.*, 2021, **11**, 1136–1178.
- 58 C. Long, J. Han, J. Guo, C. Yang, S. Liu and Z. Tang, *Chem. Catal.*, 2021, **1**, 509–522.
- 59 L. Liu, W. Li, X. He, J. Yang and N. Liu, *Small*, 2022, **18**, 2104205.
- 60 W. D. Nicoll and A. F. Smith, *Ind. Eng. Chem.*, 1955, **47**, 2548–2554.
- 61 S. Yang, A. Verdaguier-Casadevall, L. Arnarson, L. Silvioli, V. Čolić, R. Frydendal, J. Rossmeisl, I. Chorkendorff and I. E. L. Stephens, *ACS Catal.*, 2018, **8**, 4064–4081.
- 62 K. Otsuka and I. Yamanaka, *Electrochim. Acta*, 1990, **35**, 319–322.
- 63 W. Li, A. Bonakdarpour, E. Gyenge and D. P. Wilkinson, *ChemSusChem*, 2013, **6**, 2137–2143.
- 64 C. Xia, Y. Xia, P. Zhu, L. Fan and H. Wang, *Science*, 2019, **366**, 226–231.
- 65 E. Jung, H. Shin, W. Hooch Antink, Y. E. Sung and T. Hyeon, *ACS Energy Lett.*, 2020, **5**, 1881–1892.
- 66 S. Siahrostami, A. Verdaguier-Casadevall, M. Karamad, I. Chorkendorff, I. E. L. Stephens and J. Rossmeisl, *ECS Trans.*, 2013, **58**, 53–62.
- 67 P. J. Ferreira, G. J. la O', Y. Shao-Horn, D. Morgan, R. Makharia, S. Kocha and H. A. Gasteiger, *J. Electrochem. Soc.*, 2005, **152**, A2256.
- 68 S. Cherevko, G. P. Keeley, S. Geiger, A. R. Zerodjanin, N. Hodnik, N. Kulyk and K. J. J. Mayrhofer, *ChemElectroChem*, 2015, **2**, 1471–1478.
- 69 N. Seselj, S. M. Alfaro, E. Bompolaki, L. N. Cleemann, T. Torres and K. Azizi, *Adv. Mater.*, 2023, **35**, 1–28.
- 70 F. D. Speck, J. H. Kim, G. Bae, S. H. Joo, K. J. J. Mayrhofer, C. H. Choi and S. Cherevko, *JACS Au*, 2021, **1**, 1086–1100.
- 71 J. Zhao, X. Huang, H. Chang, S. Hwa Chan and Z. Tu, *Energy Convers. Manage.: X*, 2021, **10**, 100087.
- 72 T. Engl, L. Gubler and T. J. Schmidt, *Energy Technol.*, 2016, **4**, 65–74.
- 73 M. Ledendecker, J. S. Mondschein, O. Kasian, S. Geiger, D. Göhl, M. Schalenbach, A. Zerodjanin, S. Cherevko, R. E. Schaak and K. Mayrhofer, *Angew. Chem., Int. Ed.*, 2017, **56**, 9767–9771.
- 74 H. Cheng, J. Wang, C. Wu and Z. Liu, *Energy Mater. Adv.*, 2023, **4**, 1–26.
- 75 T. Imhof, R. K. F. Della Bella, B. M. Stühmeier, H. A. Gasteiger and M. Ledendecker, *Phys. Chem. Chem. Phys.*, 2023, **25**, 20533–20545.
- 76 T. Lochner, R. M. Kluge, J. Fichtner, H. A. El-Sayed, B. Garlyyev and A. S. Bandarenka, *ChemElectroChem*, 2020, **7**, 3545–3568.
- 77 A. V. Casadevall and R. Frydendal, *US Pat.*, 20190071783A1, 2019.
- 78 M. S. Kronka, G. V. Fortunato, L. Mira, A. J. dos Santos and M. R. V. Lanza, *Chem. Eng. J.*, 2023, **452**, 139598.
- 79 X. Zhou, Y. Min, C. Zhao, C. Chen, M.-K. Ke, S.-L. Xu, J.-J. Chen, Y. Wu and H.-Q. Yu, *Nat. Commun.*, 2024, **15**, 193.
- 80 T. Iwasaki, Y. Masuda, H. Ogihara and I. Yamanaka, *Electrocatalysis*, 2018, **9**, 236–242.
- 81 F. Du, J. A. Hirschfeld, X. Huang, K. Jozwiak, T. A. Dao, A. Bauer, T. J. Schmidt and A. Orfanidi, *J. Electrochem. Soc.*, 2021, **168**, 074504.
- 82 X. Bai, Q. Jian, B. Huang, L. Luo and Y. Chen, *J. Power Sources*, 2022, **520**, 230809.
- 83 Z. Xiong, B. Wen, D. Banham, S. H. Chan, Z. Xie, Y. Liang and S. Liao, *Front. Energy Res.*, 2022, **10**, 1–14.
- 84 S. H. Lee, J. C. Lin, M. Farmand, A. T. Landers, J. T. Feaster, J. E. Avilés Acosta, J. W. Beeman, Y. Ye, J. Yano, A. Mehta,



- R. C. Davis, T. F. Jaramillo, C. Hahn and W. S. Drisdell, *J. Am. Chem. Soc.*, 2021, **143**, 588–592.
- 85 W. Zhang, Q. Fu, Q. Luo, L. Sheng and J. Yang, *JACS Au*, 2021, **1**, 2130–2145.
- 86 X. Liu, J. Meng, J. Zhu, M. Huang, B. Wen, R. Guo and L. Mai, *Adv. Mater.*, 2021, **33**, 1–34.
- 87 E. S. Koh, S. Geiger, A. Gunnarson, T. Imhof, G. M. Meyer, P. Paciok, B. J. M. Etzold, M. Rose, F. Schüth and M. Ledendecker, *ChemElectroChem*, 2023, **10**, e202200924.
- 88 M. Abdollahi and A. Hosseini, *Encyclopedia of Toxicology*, Elsevier, 3rd edn, 2014, vol. 2, pp. 967–970.
- 89 J. Leifeld and I. Kögel-Knabner, *Soil Biol. Biochem.*, 2001, **33**, 2155–2158.
- 90 E. Brillas, I. Sirés and M. A. Oturan, *Chem. Rev.*, 2009, **109**, 6570–6631.
- 91 E. Brillas, *Chemosphere*, 2020, **250**, 126198.
- 92 A. J. Bard, R. Parsons and J. Jordan, *Standard Potentials in Aqueous Solution*, CRC Press, UK, 1985.
- 93 J. Weinstein and B. H. J. Bielski, *J. Am. Chem. Soc.*, 1979, **101**, 58–62.
- 94 S. Gligorovski, R. Strekowski, S. Barbati and D. Vione, *Chem. Rev.*, 2015, **115**, 13051–13092.
- 95 W. Xing, G. Lalwani, I. Rusakova and B. Sitharaman, *Part. Part. Syst. Charact.*, 2014, **31**, 745–750.
- 96 T. Du, A. S. Adeleye, T. Zhang, N. Yang, R. Hao, Y. Li, W. Song and W. Chen, *Environ. Sci.: Nano*, 2019, **6**, 2484–2494.
- 97 E. Kuhnert, V. Hacker and M. Bodner, *Int. J. Energy Res.*, 2023, **2023**, 3183108.
- 98 C. K. Duesterberg, S. E. Mylon and T. D. Waite, *Environ. Sci. Technol.*, 2008, **42**, 8522–8527.
- 99 S. A. Walling, W. Um, C. L. Corkhill and N. C. Hyatt, *npj Mater. Degrad.*, 2021, **5**, 1–20.
- 100 S. Qiu, D. He, J. Ma, T. Liu and T. D. Waite, *Electrochim. Acta*, 2015, **176**, 51–58.
- 101 L. Gubler, S. M. Dockheer and W. H. Koppenol, *ECS Meet. Abstr.*, 2011, **MA2011-02**, 1141.
- 102 U. Martinez, S. Komini Babu, E. F. Holby, H. T. Chung, X. Yin and P. Zelenay, *Adv. Mater.*, 2019, **31**, 1–20.
- 103 E. Fajardo-Puerto, A. Elmouwahidi, E. Bailón-García, A. F. Pérez-Cadenas and F. Carrasco-Marín, *Catalysts*, 2023, **13**, 674.
- 104 A. D. Bokare and W. Choi, *J. Hazard. Mater.*, 2014, **275**, 121–135.
- 105 J. Feng, C. Chu and Z. Ma, *Electrochem. Commun.*, 2021, **125**, 106970.
- 106 S. Hussain, E. Aneggi and D. Goi, *Environ. Chem. Lett.*, 2021, **19**, 2405–2424.
- 107 N. V. Maksimchuk, J. Puiggali-Jou, O. V. Zalomaeva, K. P. Larionov, V. Y. Evtushok, I. E. Soshnikov, A. Solé-Daura, O. A. Kholdeeva, J. M. Poblet and J. J. Carbó, *ACS Catal.*, 2023, **13**, 10324–10339.
- 108 Y. Li, C. J. Miller, L. Wu and T. D. Waite, *Environ. Sci. Technol.*, 2022, **56**, 5820–5829.
- 109 H. Zeng, G. Zhang, Q. Ji, H. Liu, X. Hua, H. Xia, M. Sillanpää and J. Qu, *Environ. Sci. Technol.*, 2020, **54**, 14725–14731.
- 110 W. Zheng, Y. Liu, F. Liu, Y. Wang, N. Ren and S. You, *Water Res.*, 2022, **223**, 118994.
- 111 M. Pourbaix, *Lectures on Electrochemical Corrosion*, Springer, US, 1973.
- 112 P. Cao, X. Quan, K. Zhao, S. Chen, H. Yu and Y. Su, *Environ. Sci. Technol.*, 2020, **54**, 12662–12672.
- 113 S. Weon, D. Huang, K. Rigby, C. Chu, X. Wu and J.-H. Kim, *ACS ES&T Eng.*, 2021, **1**, 157–172.
- 114 J. Bak, H. Kim, S. J. Lee, M. J. Kim, E. J. Kim, J. H. Roh, J. W. Shin, C. H. Choi and E. A. Cho, *ACS Catal.*, 2020, **10**, 12300–12309.
- 115 D. Böhm, M. Beetz, C. Gebauer, M. Bernt, J. Schröter, M. Kornherr, F. Zoller, T. Bein and D. Fattakhova-Rohlfing, *Appl. Mater. Today*, 2021, **24**, 101134.
- 116 L. Dubau, L. Castanheira, F. Maillard, M. Chatenet, O. Lottin, G. Maranzana, J. Dillet, A. Lamibrac, J. C. Perrin, E. Moukheiber, A. Elkaddouri, G. De Moor, C. Bas, L. Flandin and N. Caqué, *Wiley Interdiscip. Rev.: Energy Environ.*, 2014, **3**, 540–560.
- 117 Y. Yu, H. Li, H. Wang, X. Z. Yuan, G. Wang and M. Pan, *J. Power Sources*, 2012, **205**, 10–23.
- 118 X. Zhang, Y. Yang, L. Guo and H. Liu, *Int. J. Hydrogen Energy*, 2017, **42**, 4699–4705.
- 119 V. Goellner, C. Baldizzone, A. Schuppert, M. T. Sougrati, K. Mayrhofer and F. Jaouen, *Phys. Chem. Chem. Phys.*, 2014, **16**, 18454–18462.
- 120 T. Kinumoto, K. Takai, Y. Iriyama, T. Abe, M. Inaba and Z. Ogumi, *J. Electrochem. Soc.*, 2006, **153**, A58.
- 121 K. Kumar, L. Dubau, M. Mermoux, J. Li, A. Zitolo, J. Nelayah, F. Jaouen and F. Maillard, *Angew. Chem., Int. Ed.*, 2020, **59**, 3235–3243.
- 122 L. Dubau, L. Castanheira, G. Berthomé and F. Maillard, *Electrochim. Acta*, 2013, **110**, 273–281.
- 123 V. Goellner, V. Armel, A. Zitolo, E. Fonda and F. Jaouen, *J. Electrochem. Soc.*, 2015, **162**, H403–H414.
- 124 K. Kumar, L. Dubau, M. Mermoux, J. Li, A. Zitolo, J. Nelayah, F. Jaouen and F. Maillard, *Angew. Chem., Int. Ed.*, 2020, **132**, 3261–3269.
- 125 S. Ünsal, R. Girod, C. Appel, D. Karpov, M. Mermoux, F. Maillard, V. A. Saveleva, V. Tileli, T. J. Schmidt and J. Herranz, *J. Am. Chem. Soc.*, 2023, **145**, 7845–7858.
- 126 X. Xie, C. He, B. Li, Y. He, D. A. Cullen, E. C. Wegener, A. J. Kropf, U. Martinez, Y. Cheng, M. H. Engelhard, M. E. Bowden, M. Song, T. Lemmon, X. S. Li, Z. Nie, J. Liu, D. J. Myers, P. Zelenay, G. Wang, G. Wu, V. Ramani and Y. Shao, *Nat. Catal.*, 2020, **3**, 1044–1054.
- 127 A. Laconti, H. Liu, C. Mittelsteadt and R. McDonald, *ECS Trans.*, 2006, **1**, 199–219.
- 128 M. Lefèvre and J. P. Dodelet, *Electrochim. Acta*, 2003, **48**, 2749–2760.
- 129 G. Zhang, R. Chenitz, M. Lefèvre, S. Sun and J. P. Dodelet, *Nano Energy*, 2016, **29**, 111–125.
- 130 C. W. Jones, in *Applications of Hydrogen Peroxide and Derivatives*, ed. J. H. Clark and M. J. Braithwaite, The Royal Society of Chemistry, 1999, pp.1–36.
- 131 L. Gubler, S. M. Dockheer and W. H. Koppenol, *J. Electrochem. Soc.*, 2011, **158**, B755–B769.



- 132 W. Kiciński and S. Dyjak, *Carbon N. Y.*, 2020, **168**, 748–845.
- 133 Y. Lum, Y. Kwon, P. Lobaccaro, L. Chen, E. L. Clark, A. T. Bell and J. W. Ager, *ACS Catal.*, 2016, **6**, 202–209.
- 134 P. T. Yu, W. Gu, J. Zhang, R. Makharia, F. T. Wagner and H. A. Gasteiger, in *Polymer Electrolyte Fuel Cell Durability*, ed. F. N. Büchi, M. Inaba and T. J. Schmidt, Springer, New York, New York, NY, 2009, pp.29–53.
- 135 W. Shi, K. H. Wu, J. Xu, Q. Zhang, B. Zhang and D. S. Su, *Chem. Mater.*, 2017, **29**, 8670–8678.
- 136 C. Poidevin and A. A. Auer, *Carbon N. Y.*, 2021, **171**, 618–633.
- 137 K. Ono, Y. Yasuda, K. Sekizawa, N. Takeuchi, T. Yoshida and M. Sudoh, *Electrochim. Acta*, 2013, **97**, 58–65.
- 138 C. Poidevin, P. Paciok, M. Heggen and A. A. Auer, *J. Chem. Phys.*, 2019, **150**, 041705.
- 139 Y. Qi, Y. Huang, Z. Gao, C. H. Chen, A. Perego, H. Yildirim, M. Odgaard, T. Asset, P. Atanassov and I. V. Zenyuk, *J. Power Sources*, 2022, **551**, 232209.
- 140 S. Vinod Selvaganesh, G. Selvarani, P. Sridhar, S. Pitchumani and A. K. Shukla, *Fuel Cells*, 2011, **11**, 372–384.
- 141 C. H. Choi, H. K. Lim, M. W. Chung, G. Chon, N. Ranjbar Sahraie, A. Altin, M. T. Sougrati, L. Stievano, H. S. Oh, E. S. Park, F. Luo, P. Strasser, G. Dražić, K. J. J. Mayrhofer, H. Kim and F. Jaouen, *Energy Environ. Sci.*, 2018, **11**, 3176–3182.
- 142 Y. Hashimasa, T. Numata, K. Moriya and S. Watanabe, *J. Power Sources*, 2006, **155**, 182–189.
- 143 J. S. Spindelov and D. C. Papageorgopoulos, *Fuel Cells*, 2011, **11**, 775–786.
- 144 S. Stariha, N. Macauley, B. T. Sneed, D. Langlois, K. L. More, R. Mukundan and R. L. Borup, *J. Electrochem. Soc.*, 2018, **165**, F492–F501.
- 145 S. Chen, Z. Wei, L. Guo, W. Ding, L. Dong, P. Shen, X. Qi and L. Li, *Chem. Commun.*, 2011, **47**, 10984–10986.
- 146 X. Huang, M. Song, J. Zhang, T. Shen, G. Luo and D. Wang, *Nano-Micro Lett.*, 2023, **15**, 86.

